

## Structural Basis of Catalysis and Inhibition of HDAC6 CD1, the Enigmatic Catalytic Domain of Histone Deacetylase 6

Jeremy D. Osko, and David W. Christianson

*Biochemistry*, **Just Accepted Manuscript** • DOI: 10.1021/acs.biochem.9b00934 • Publication Date (Web): 22 Nov 2019

Downloaded from [pubs.acs.org](https://pubs.acs.org) on November 23, 2019

### Just Accepted

“Just Accepted” manuscripts have been peer-reviewed and accepted for publication. They are posted online prior to technical editing, formatting for publication and author proofing. The American Chemical Society provides “Just Accepted” as a service to the research community to expedite the dissemination of scientific material as soon as possible after acceptance. “Just Accepted” manuscripts appear in full in PDF format accompanied by an HTML abstract. “Just Accepted” manuscripts have been fully peer reviewed, but should not be considered the official version of record. They are citable by the Digital Object Identifier (DOI®). “Just Accepted” is an optional service offered to authors. Therefore, the “Just Accepted” Web site may not include all articles that will be published in the journal. After a manuscript is technically edited and formatted, it will be removed from the “Just Accepted” Web site and published as an ASAP article. Note that technical editing may introduce minor changes to the manuscript text and/or graphics which could affect content, and all legal disclaimers and ethical guidelines that apply to the journal pertain. ACS cannot be held responsible for errors or consequences arising from the use of information contained in these “Just Accepted” manuscripts.

1  
2  
3 **Structural Basis of Catalysis and Inhibition of HDAC6 CD1, the**  
4  
5  
6 **Enigmatic Catalytic Domain of Histone Deacetylase 6**  
7  
8  
9  
10  
11  
12  
13  
14  
15  
16  
17  
18

19 Jeremy D. Osko<sup>1</sup> and David W. Christianson<sup>1,\*</sup>  
20  
21  
22  
23  
24  
25  
26  
27  
28  
29

30 <sup>1</sup>Roy and Diana Vagelos Laboratories, Department of Chemistry, University of Pennsylvania,  
31  
32 231 South 34<sup>th</sup> Street, Philadelphia, PA 19104-6323, United States  
33  
34  
35  
36  
37  
38  
39  
40  
41  
42  
43  
44  
45  
46  
47  
48  
49

50 \*author to whom correspondence should be sent: E-mail [chris@sas.upenn.edu](mailto:chris@sas.upenn.edu)  
51  
52  
53  
54  
55  
56  
57  
58  
59  
60

**Abstract**

1  
2  
3  
4  
5  
6  
7  
8  
9  
10  
11  
12  
13  
14  
15  
16  
17  
18  
19  
20  
21  
22  
23  
24  
25  
26  
27  
28  
29  
30  
31  
32  
33  
34  
35  
36  
37  
38  
39  
40  
41  
42  
43  
44  
45  
46  
47  
48  
49  
50  
51  
52  
53  
54  
55  
56  
57  
58  
59  
60

Histone deacetylase 6 (HDAC6) is emerging as a target for inhibition in therapeutic strategies aimed at treating cancer, neurodegenerative disease, and other disorders. Among the metal-dependent HDAC isozymes, HDAC6 is unique in that it contains two catalytic domains, CD1 and CD2. CD2 is a tubulin deacetylase and a tau deacetylase, and the development of HDAC6-selective inhibitors has focused exclusively on this domain. In contrast, there is a dearth of structural and functional information regarding CD1, which exhibits much narrower substrate specificity in comparison with CD2. As the first step in addressing the CD1 information gap, we now present X-ray crystal structures of seven inhibitor complexes with wild-type, Y363F, and K330L HDAC6 CD1. These structures broaden our understanding of molecular features important for catalysis and inhibitor binding. The active site of HDAC6 CD1 is wider than that of CD2, which is unexpected in view of the narrow substrate specificity of CD1. Amino acid substitutions between HDAC6 CD1 and CD2, as well as conformational differences in conserved residues, define striking differences in active site contours. Catalytic activity measurements with HDAC6 CD1 confirm the preference for peptide substrates containing C-terminal acetyllysine residues. However, these measurements also show that CD1 exhibits weak activity for peptide substrates bearing certain small amino acids on the carboxyl side of the scissile acetyllysine residue. Taken together, these results establish a foundation for understanding the structural basis of HDAC6 CD1 catalysis and inhibition, pointing to possible avenues for the development of HDAC6 CD1-selective inhibitors.

## INTRODUCTION

The metal-dependent histone deacetylases (HDACs) serve critical roles in the regulation of protein function by catalyzing the hydrolysis of acetyllysine side chains to generate lysine and acetate.<sup>1-4</sup> Lysine acetylation-deacetylation cycles are implicated in a wide variety of biological processes such as metabolism,<sup>5,6</sup> cell signaling,<sup>7</sup> and epigenetics,<sup>8,9</sup> so the facile deacetylation of acetyllysine is critically important in the chemistry of the cell. Notably, the disruption of balanced acetylation-deacetylation cycles is associated with certain pathologies, such as cancer and neurodegenerative disease.<sup>10,11</sup> The development and use of HDAC inhibitors to modulate acetylation-deacetylation cycles has been a validated therapeutic strategy<sup>10-14</sup> ever since the approval of suberoylanilide hydroxamic acid (SAHA, formulated as Vorinostat) for the treatment of cutaneous T-cell lymphoma in 2006.<sup>15-17</sup>

Consisting of a single polypeptide chain of 1215 amino acids, human histone deacetylase 6 (HDAC6; Uniprot Q9UBN7) is the largest member of the metal-dependent HDAC family.<sup>18,19</sup> HDAC6 is unique among the greater HDAC family in that it contains two catalytic domains,<sup>19-21</sup> designated CD1 and CD2, in addition to a ubiquitin binding domain.<sup>22</sup> Residues important for the chemistry of catalysis are conserved in both catalytic domains, including Zn<sup>2+</sup> ligands, tandem histidine residues serving general base-general acid functions, and a tyrosine residue that assists the Zn<sup>2+</sup> ion in polarizing the scissile carbonyl of acetyllysine for nucleophilic attack by a Zn<sup>2+</sup>-bound solvent molecule.<sup>4,23-25</sup>

While CD2 functions to catalyze the deacetylation of cytosolic protein substrates such as  $\alpha$ -tubulin<sup>26,27</sup> and Tau,<sup>28-30</sup> the catalytic function of CD1 is more enigmatic. Initial studies demonstrated that both CD1 and CD2 exhibited activity in the deacetylation of histone substrates, but only CD2 exhibited tubulin deacetylase activity, suggesting alternate substrate specificities for each catalytic domain.<sup>19,31</sup> Additional studies suggested that both domains were required for deacetylase activity,<sup>32</sup> but only CD2 was catalytically active.<sup>33</sup> Curiously, a more

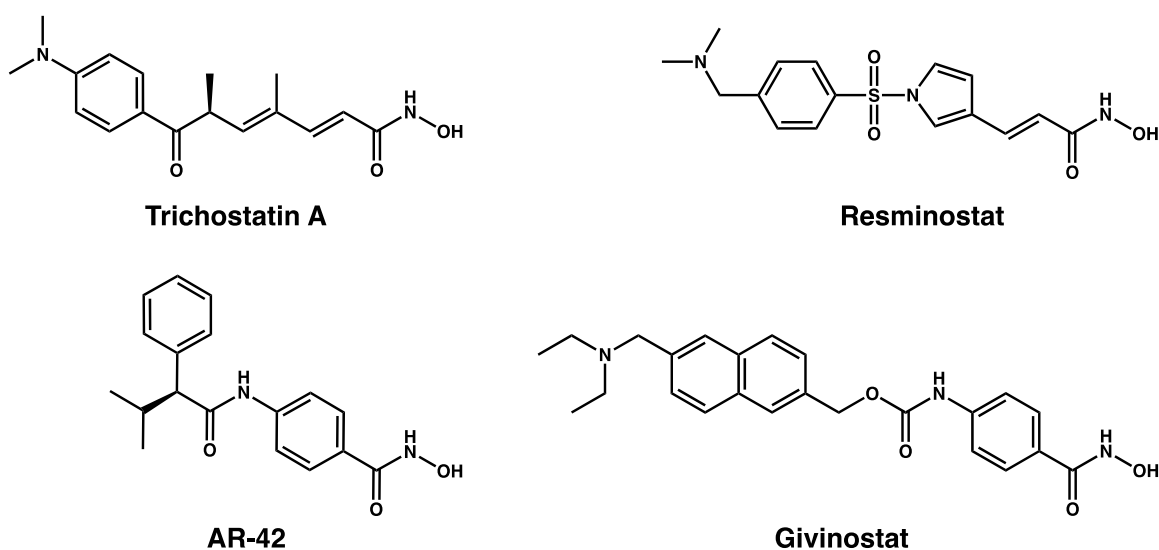
1  
2  
3 recent report suggested that CD1 is an E3 ubiquitin ligase,<sup>34</sup> and an even more recent report  
4 suggested that CD1 deacetylates the RNA helicase DDX3X.<sup>35</sup> However, these measurements  
5 were made in cell extracts and not purified enzymes, so the structural mechanistic bases of  
6 these activities are not established.  
7  
8  
9  
10

11  
12 Recombinant expression of protein constructs corresponding to individual CD1 and CD2  
13 domains of human and zebrafish HDAC6 conclusively demonstrated that both catalytic domains  
14 exhibit lysine deacetylase activity.<sup>36</sup> However, the CD1 domain exhibits very narrow specificity  
15 for peptide substrates containing a C-terminal acetyllysine residue. A free  $\alpha$ -carboxylate group  
16 appears to enable substrate binding in the CD1 active site due to the presence of a  
17 “gatekeeper” residue, K330 (zebrafish HDAC6 CD1 numbering; Uniprot F8W4B7), that is unique  
18 to HDAC6 CD1 orthologs. This residue appears as a leucine in other HDAC isozymes except for  
19 HDAC8, where it is a methionine, and HDAC10, where it is a glutamate.  
20  
21  
22  
23  
24  
25  
26  
27  
28

29 The X-ray crystal structures of HDAC6 CD2 from *Homo sapiens* (human),<sup>36</sup> and HDAC6  
30 CD1 and CD2 from *Danio rerio* (zebrafish)<sup>36,37</sup> were recently reported. Since then, numerous  
31 crystal structures of HDAC6 CD2-inhibitor complexes have illuminated active site features  
32 contributing to isozyme-selective inhibition.<sup>38-43</sup> However, although more than 50 crystal  
33 structures of HDAC6 CD2-inhibitor complexes have been reported to date, the structures of only  
34 2 different HDAC6 CD1-inhibitor complexes are currently available.<sup>36,37</sup> Given the observed  
35 structural differences between the active site clefts of HDAC6 CD1 and CD2,<sup>36,37</sup> as well as the  
36 conclusive determination of catalytic activity and narrow substrate specificity for HDAC6 CD1,<sup>36</sup>  
37 an understanding of inhibitor binding determinants in the active site of this unusual domain is  
38 needed to inform the design and evaluation of selective high-affinity inhibitors. In turn, such  
39 inhibitors might be useful for probing the biological function of HDAC6 CD1.  
40  
41  
42  
43  
44  
45  
46  
47  
48  
49  
50  
51  
52

53 To address this dearth of structural information, we now report seven new crystal  
54 structures of HDAC6 CD1-inhibitor complexes. Inhibitor structures are illustrated in Figure 1.  
55  
56  
57  
58  
59  
60

1  
2  
3 These structures include complexes formed with wild-type, K330L, or Y363F HDAC6 CD1  
4 (Y363 is the catalytic tyrosine). Additionally, we report catalytic activity measurements of  
5 HDAC6 CD1 with a series of acetyllysine-containing peptide substrates. While we previously  
6 demonstrated that HDAC6 CD1 cannot readily tolerate alanine or proline residues following the  
7 scissile acetyllysine residue,<sup>36</sup> we show here that HDAC6 CD1 exhibits low catalytic activity with  
8 substrates containing other small residues following the scissile acetyllysine. Even so, maximal  
9 catalytic activity is observed only for substrates bearing a free  $\alpha$ -carboxylate group.  
10  
11  
12  
13  
14  
15  
16  
17



36  
37  
38  
39  
40  
41  
42  
43  
44  
45  
46  
47  
48  
49  
50  
51  
52  
53  
54  
55  
56  
57  
58  
59  
60

**Figure 1.** Inhibitors studied in complexes with HDAC6 CD1.

## MATERIALS AND METHODS

**Reagents.** In general, all chemicals were purchased from Fisher Scientific, Millipore Sigma, or Hampton Research and used without further purification. Trichostatin A was purchased from Millipore Sigma. Resminostat and (S)-N-hydroxy-4-(3-methyl-2-phenylbutanamido)-benzamide (AR-42) were purchased from Selleck Chemicals. Givinostat was purchased from Tocris Bioscience.

**Protein purification.** HDAC6 CD1 from *D. rerio* (henceforth simply HDAC6 CD1) was recombinantly expressed using a pET-28a(+) vector by Genscript. This construct utilizes a

1  
2  
3 NdeI/BAMHI cloning site and contains kanamycin bacterial resistance. By nature of the pET-  
4 28a(+) vector, a His tag is located at both the N-terminus and C-terminus with an N-terminal  
5 thrombin cleavage site. This procedure differs from that initially reported by Hai and  
6  
7 Christianson.<sup>36</sup>  
8  
9

10  
11 Protein was expressed using *Escherichia coli* One Shot BL21(DE3) cells (Invitrogen)  
12 and grown in 2xYT medium in the presence of 50 µg/mL ampicillin. Cells were grown at 37° C  
13 and 250 RPM in an Innova 40 incubator shaker until OD<sub>600</sub> reached approximately 0.80. The  
14 temperature was then reduced to 18° C until OD<sub>600</sub> reached 1.0. At this point, cells were  
15 supplemented with 400 µM isopropyl β-L-1-thiogalactopyranoside (IPTG; Gold Biotechnology)  
16 and were grown for an additional 18 h at 250 RPM. Finally, cells were centrifuged for 20 min at  
17 5,000 RPM using a Sorvall LYNX 6000 centrifuge and cell pellets were stored at -80° C until  
18 further use.  
19  
20  
21  
22  
23  
24  
25  
26  
27

28  
29 The cell pellet was thawed and re-suspended in 100 mL of Buffer A [50 mM K<sub>2</sub>HPO<sub>4</sub> (pH  
30 8.0), 1 mM tris(2-carboxyethyl)phosphine (TCEP), 300 mM NaCl, 30 mM imidazole, 5%  
31 glycerol]. Additionally, 2 protease inhibitor tablets, 0.1 mg/mL lysozyme, and 50 µg/mL DNAse  
32 were added to the solution. The cells were then lysed by sonication. Cell lysate was centrifuged  
33 for 1 h at 15,000 RPM using a Sorval LYNX 6000 centrifuge and then applied to a 5-mL pre-  
34 equilibrated HisTrap HP column.  
35  
36  
37  
38  
39  
40  
41

42 The His-tagged HDAC6 CD1 protein bound to the HisTrap HP column and was eluted  
43 using Buffer B [50 mM K<sub>2</sub>HPO<sub>4</sub> (pH 8.0), 1 mM TCEP, 300 mM NaCl, 300 mM imidazole, 5%  
44 glycerol]. The CD1-containing fractions were concentrated to 5 mL using a 15-mL centrifugal  
45 filter unit with a molecular weight cut-off of 10 kDa. The protein was then filtered using a 0.22-  
46 µm Millex-GV filter unit prior to being loaded onto a HiLoad Superdex 26/600 200 pg column.  
47 The column was pre-equilibrated with 360 mL of Buffer C [50 mM 4-(2-hydroxyethyl)piperazine-  
48 1-ethanesulfonic acid (HEPES) (pH 7.5), 100 mM KCl, 1 mM TCEP, 5% glycerol]. The 5-mL  
49  
50  
51  
52  
53  
54  
55  
56  
57  
58  
59  
60

1  
2  
3 sample of CD1 was injected at a rate of 1 mL/min, and 5-mL fractions were collected. Pure CD1  
4  
5 protein was confirmed by SDS-PAGE, concentrated to approximately 10 mg/mL, and stored at -  
6  
7 80° C.  
8  
9

10 **Catalytic activity measurements.** To measure the rate of lysine deacetylation  
11 catalyzed by CD1, a discontinuous liquid chromatography-mass spectrometry (LC-MS) assay  
12 was implemented as previously established for HDAC6.<sup>36</sup> Upon deacetylation of the  
13  
14 acetyllysine-containing peptide substrate by HDAC6 CD1 and incubation with dansyl chloride,  
15  
16 the liberated primary amino group of product lysine is dansylated and thereby enables detection  
17  
18 and quantification using LC-MS. No mass shift indicates no activity.  
19  
20  
21  
22

23 To briefly summarize the procedure, 5  $\mu$ L of HDAC6 CD1 (final enzyme concentration =  
24 1  $\mu$ M) in assay buffer [20 mM HEPES (pH 7.5), 100 mM NaCl, 5 mM KCl, 1 mM  $MgCl_2$ ] was  
25  
26 combined with 35  $\mu$ L of substrate solution (final substrate concentration = 1 mM). After 60 min  
27  
28 at 25°C, each reaction was quenched with 10  $\mu$ L of  $NaHCO_3$  (1.6 M, pH 10.0) and 40  $\mu$ L dansyl  
29  
30 chloride (10 mM in acetonitrile). Each reaction mixture was allowed to equilibrate for 60 min at  
31  
32 50 °C, after which it was analyzed by LC-MS using a Waters SQD equipped with an Acquity  
33  
34 UPLC (Waters, Milford, MA, USA). Specific activities were calculated using a standard curve.  
35  
36 Assays were run in triplicate.  
37  
38  
39  
40

41 **Crystallization.** All HDAC6 CD1-inhibitor complexes were crystallized by the sitting-drop  
42 vapor diffusion method using a Mosquito crystallization robot (TTP Labtech). Typically, a 100-nL  
43  
44 drop of protein solution [10 mg/mL HDAC6 CD1, 50 mM HEPES (pH 7.5), 100 mM KCl, 5%  
45  
46 glycerol (v/v), 1 mM TCEP, and 2 mM inhibitor] was added to a 100-nL drop of precipitant  
47  
48 solution and equilibrated against 80  $\mu$ L of precipitant solution in the well reservoir. Prior to flash-  
49  
50 cooling, all crystals were soaked with 20% ethylene glycol for cryoprotection. All complexes  
51  
52 were crystallized at 4 °C. X-ray diffraction data were collected on Northeastern Collaborative  
53  
54  
55  
56  
57  
58  
59  
60

1  
2  
3 Access Team (NE-CAT) beamlines 24-ID-C and 24-ID-E at the Advanced Photon Source  
4  
5 (APS).  
6  
7

8 For cocrystallization of the HDAC6 CD1–Trichostatin A complex, the precipitant solution  
9  
10 was 0.2 M ammonium tartrate dibasic (pH 7.0) and 20% PEG 3350. For cocrystallization of the  
11  
12 HDAC6 CD1–AR-42 complex, the precipitant solution was 0.2 M ammonium tartrate dibasic (pH  
13  
14 7.0) and 20% PEG 3350. For cocrystallization of the Y363F HDAC6 CD1–Trichostatin A  
15  
16 complex, the precipitant solution was 0.2 M sodium malonate (pH 7.0) and 20% PEG 3350. For  
17  
18 cocrystallization of the Y363F HDAC6 CD1–AR-42 complex, the precipitant solution was 0.2 M  
19  
20 sodium phosphate dibasic dihydride and 20% PEG 3350. For cocrystallization of the K330L  
21  
22 HDAC6 CD1–AR-42 complex, the precipitant solution was 0.2 M magnesium formate dihydrate  
23  
24 and 20% w/v PEG 3350. For cocrystallization of the K330L HDAC6 CD1–Resminostat complex,  
25  
26 the precipitant solution was 0.1 M ammonium citrate tribasic (pH 7.0) and 12% w/v PEG 3350.  
27  
28 For cocrystallization of the K330L HDAC6 CD1–Givinostat complex, the precipitant solution was  
29  
30 0.2 M magnesium formate dihydrate and 20% w/v PEG 3350.  
31  
32

33 **Data reduction, phasing, and structure refinement.** The CCP4 program suite<sup>44</sup> was  
34  
35 used for data reduction. Data were indexed using the CCP4 program iMosflm<sup>45</sup> while Aimless<sup>46</sup>  
36  
37 was utilized for data scaling. The initial electron density map of each enzyme-inhibitor complex  
38  
39 was phased by molecular replacement using the atomic coordinates of HDAC6 CD1 (PDB  
40  
41 5EEF)<sup>36</sup> as a search probe with Phaser.<sup>47</sup> The interactive graphics program Coot<sup>48</sup> was used to  
42  
43 build and manipulate atomic models of each enzyme-inhibitor complex. Crystallographic  
44  
45 refinement was performed using Phenix.<sup>49</sup> Final refined structures were validated using  
46  
47 MolProbity<sup>50</sup> prior to deposition in the Protein Data Bank ([www.rcsb.org](http://www.rcsb.org)). All data collection,  
48  
49 reduction, and refinement statistics are recorded in Table 1.  
50  
51  
52  
53  
54  
55  
56  
57  
58  
59  
60

**Table 1.** Data Collection and Refinement Statistics for HDAC6 CD1–Inhibitor Complexes<sup>a</sup>

	HDAC6 CD1– Trichostatin A	HDAC6 CD1– AR-42	Y363F HDAC6 CD1– Trichostatin A	Y363F HDAC6 CD1–AR-42	K330L HDAC6 CD1–AR-42	K330L HDAC6 CD1– Resminostat	K330L HDAC6 CD1–Givinostat
<b>Data collection</b>							
<b>Space group</b>	P 2 <sub>1</sub>	P 2 <sub>1</sub> 2 <sub>1</sub> 2 <sub>1</sub>	P 2 <sub>1</sub>	P 2 <sub>1</sub> 2 <sub>1</sub> 2 <sub>1</sub>	P 2 <sub>1</sub> 2 <sub>1</sub> 2 <sub>1</sub>	P 2 <sub>1</sub> 2 <sub>1</sub> 2 <sub>1</sub>	P 2 <sub>1</sub> 2 <sub>1</sub> 2 <sub>1</sub>
<b>a,b,c (Å)</b>	53.0 124.2 55.5	54.7 61.0 121.6	52.8 124.4 55.6	54.5 60.5 121.9	55.0 60.6 121.8	67.2 102.6 112.9	55.1 60.4 122.1
<b>α,β,γ (°)</b>	90.0 114.0 90.0	90.0 90.0 90.0	90.0 114.4 90.0	90.0 90.0 90.0	90.0 90.0 90.0	90.0 90.0 90.0	90.0 90.0 90.0
<b>R<sub>merge</sub><sup>b</sup></b>	0.064 (0.546)	0.140 (0.995)	0.076 (0.578)	0.052 (0.747)	0.075 (0.222)	0.145 (2.032)	0.094 (0.359)
<b>R<sub>pim</sub><sup>c</sup></b>	0.041 (0.350)	0.062 (0.445)	0.048 (0.378)	0.022 (0.316)	0.032 (0.094)	0.062 (0.880)	0.040 (0.150)
<b>CC<sub>1/2</sub><sup>d</sup></b>	0.997 (0.753)	0.986 (0.776)	0.995 (0.731)	1.000 (0.872)	0.996 (0.977)	0.997 (0.502)	0.995 (0.952)
<b>Redundancy</b>	3.4 (3.4)	6.0 (5.8)	3.5 (3.1)	6.6 (6.5)	6.5 (6.6)	6.5 (6.2)	6.5 (6.7)
<b>Completeness (%)</b>	99.1 (98.6)	99.7 (99.8)	94.5 (87.9)	99.9 (99.3)	100.0 (99.9)	99.8 (99.6)	99.7 (99.7)
<b>I/σ</b>	9.9 (2.0)	7.2 (2.0)	10.1 (1.8)	19.2 (2.2)	15.2 (6.8)	9.8 (1.9)	12.4 (5.6)
<b>Refinement</b>							
<b>Resolution (Å)</b>	50.6-1.65 (1.70-1.65)	43.0-1.09 (1.12-1.09)	62.2-1.27 (1.31-1.27)	54.2-1.44 (1.49-1.44)	42.9-1.40 (1.44-1.40)	50.3-1.58 (1.63-1.58)	42.9-1.40 (1.45-1.40)
<b>No. reflections</b>	77846 (7694)	169488 (16796)	162601 (15378)	73857 (7242)	81863 (8131)	106860 (10560)	80865 (7985)
<b>R<sub>work</sub>/R<sub>free</sub><sup>e</sup></b>	0.187/0.222 (0.267/0.301)	0.183/0.190 (0.275/0.282)	0.182/0.196 (0.264/0.269)	0.174/0.196 (0.258/0.271)	0.166/0.184 (0.195/0.234)	0.184/0.208 (0.252/0.286)	0.152/0.169 (0.166/0.198)
<b>No. atoms<sup>f</sup></b>							
<b>Protein</b>	5466	2856	5536	2816	2843	5603	2880
<b>Ligand</b>	50	38	50	30	26	90	46
<b>Solvent</b>	193	415	563	266	384	497	432
<b>Average B factors (Å<sup>2</sup>)</b>							
<b>Protein</b>	25	13	17	20	15	19	13
<b>Ligand</b>	29	15	17	22	13	27	22
<b>Solvent</b>	28	25	27	30	27	29	27
<b>R.m.s. deviations</b>							
<b>Bond lengths (Å)</b>	0.006	0.004	0.005	0.005	0.004	0.006	0.004
<b>Bond angles (°)</b>	0.81	0.83	0.77	0.80	0.81	0.85	0.82
<b>Ramachandran plot<sup>g</sup></b>							
<b>Favored</b>	97.04	97.20	96.90	96.35	97.19	96.06	97.19
<b>Allowed</b>	2.96	2.80	3.10	3.65	2.81	3.80	2.81
<b>Outliers</b>	0.00	0.00	0.00	0.00	0.00	0.10	0.00

<sup>a</sup>Values in parentheses refer to the highest-resolution shell indicated. <sup>b</sup> $R_{\text{merge}} = \frac{\sum_{hkl} \sum_i |I_{i,hkl} - \langle I \rangle_{hkl}|}{\sum_{hkl} \sum_i I_{i,hkl}}$ , where  $\langle I \rangle_{hkl}$  is the average intensity calculated for reflection  $hkl$  from replicate measurements. <sup>c</sup> $R_{\text{p.i.m.}} = \frac{(\sum_{hkl} (1/(N-1))^{1/2} \sum_i |I_{i,hkl} - \langle I \rangle_{hkl}|)}{\sum_{hkl} \sum_i I_{i,hkl}}$ , where  $\langle I \rangle_{hkl}$  is the average intensity calculated for reflection  $hkl$  from replicate measurements and  $N$  is the number of reflections. <sup>d</sup>Pearson correlation coefficient between random half-datasets. <sup>e</sup> $R_{\text{work}} = \frac{\sum ||F_o| - |F_c||}{\sum |F_o|}$  for

1  
2  
3 reflections contained in the working set.  $|F_o|$  and  $|F_c|$  are the observed and calculated structure factor amplitudes, respectively.  $R_{free}$  is calculated using the same  
4 expression for reflections contained in the test set held aside during refinement. <sup>†</sup>Per asymmetric unit. <sup>‡</sup>Calculated with MolProbity.  
5  
6  
7  
8  
9  
10  
11  
12  
13  
14  
15  
16  
17  
18  
19  
20  
21  
22  
23  
24  
25  
26  
27  
28  
29  
30  
31  
32  
33  
34  
35  
36  
37  
38  
39  
40  
41  
42  
43  
44  
45  
46  
47

## RESULTS

**Crystal structure determinations.** The 1.65 Å-resolution crystal structure of the HDAC6 CD1–Trichostatin A complex reported herein crystallizes in monoclinic space group  $P2_1$  and is isomorphous with the previously reported crystal structure of this complex determined at lower (2.15 Å) resolution. There are no major conformation differences between these two structures, and the root-mean-square deviation (rmsd) is 0.20 Å for 306 C $\alpha$  atoms in monomer A. The simplified HDAC6 CD1 construct used in the current study represents a significant improvement over previously reported constructs in terms of the 0.5 Å-resolution improvement in the diffraction quality of crystals compared with HDAC6 CD1 derived from the fusion prepared with maltose binding protein.<sup>36</sup> Additionally, the simplified construct does not undergo slow proteolysis as observed for the CD1-CD2 didomain construct expressed in baculovirus-infected Sf9 cells.<sup>37</sup> The improved expression and purification scheme for HDAC6 CD1 consistently yields large quantities of pure protein that is more amenable to crystallization experiments.

Inhibitor binding interactions are identical in the 1.65 Å resolution structure and the 2.15 Å resolution structure. Briefly, the catalytic Zn<sup>2+</sup> ion is chelated by the inhibitor hydroxamate group with bidentate coordination geometry (Figure 2a). The Zn<sup>2+</sup>-bound hydroxamate C=O group also accepts a hydrogen bond from Y363, while the Zn<sup>2+</sup>-bound hydroxamate N–O<sup>-</sup> group accepts a hydrogen bond from H192. The hydroxamate NH group also donates a hydrogen bond to H193. Interestingly, electron density corresponding to the side chain of gatekeeper residue K330 is poor in the 1.65 Å resolution structure, so the side chain of this residue is not modeled beyond the C $\beta$  atom. This contrasts with the 2.15 Å resolution structure, in which the amino group of the K330 side chain donates a hydrogen bond to the ketone carbonyl of the inhibitor.

Differences in the binding conformation of Trichostatin A to HDAC6 CD1 and CD2 have been noted previously in the first structure determinations of HDAC6,<sup>36,37</sup> and these differences

are maintained in view of the 1.65 Å-resolution structure of the HDAC6 CD1–Trichostatin A complex reported herein and the 1.05 Å-resolution structure of the HDAC6 CD2–Trichostatin A complex recently reported by Porter and colleagues (PDB 5WGI) (Figure 2b).<sup>38</sup> Differences in the protein structure are largely confined to W78, the side chain of which moves toward the bound inhibitor in the HDAC6 CD1 complex. Differences in inhibitor binding are manifest in a ~4 Å-shift of the dimethylaminophenyl capping group toward W78.

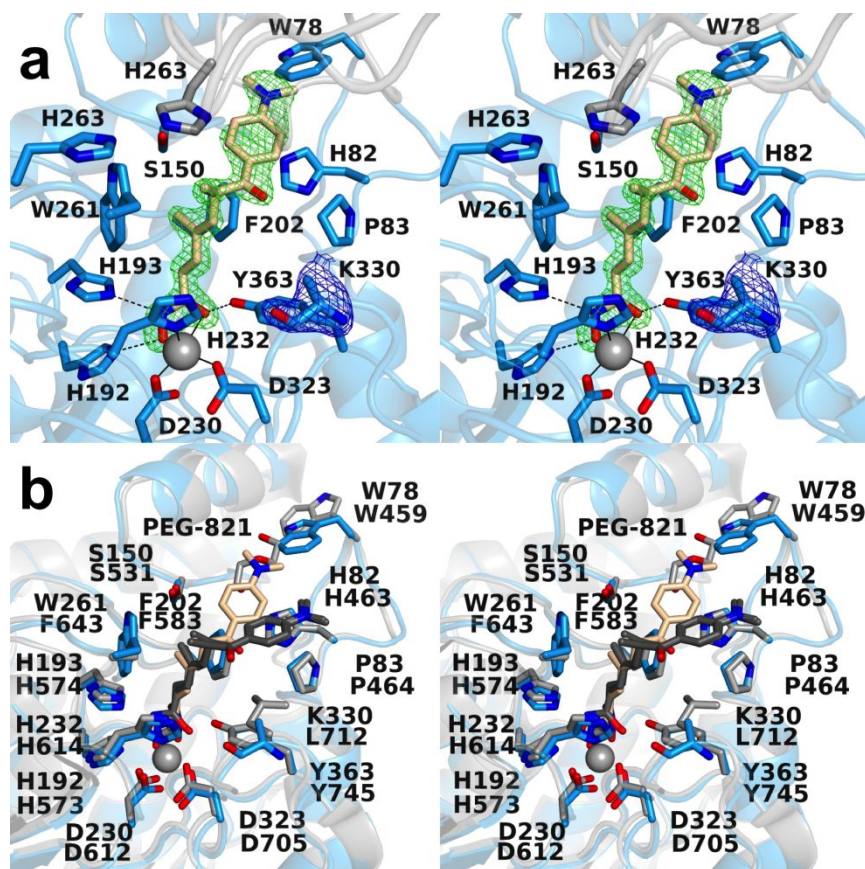
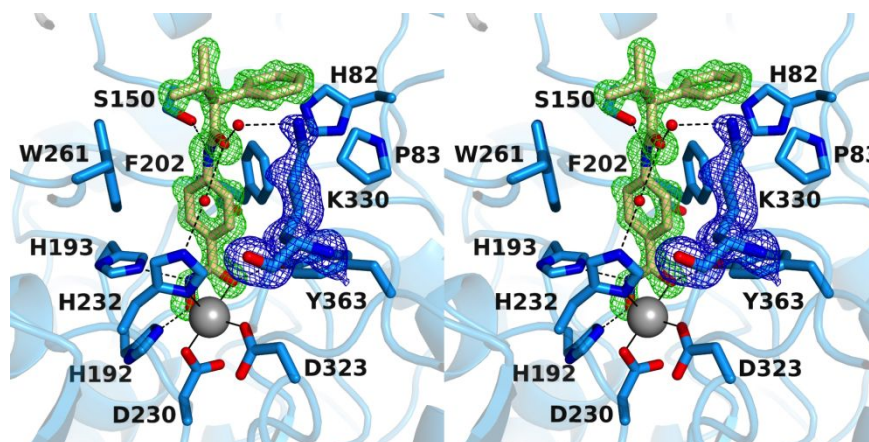


**Figure 2.** (a) Polder omit maps of the HDAC6 CD1–Trichostatin A complex (PDB 6UO2; monomer B, inhibitor contoured at 5.5  $\sigma$ ; K330 is contoured at 3.5  $\sigma$ ). Atoms are color-coded as follows: C = light blue (monomer B), light gray (monomer A), or wheat (inhibitor), N = blue, O = red, and Zn<sup>2+</sup> = gray sphere. Metal coordination and hydrogen bond interactions are indicated by solid and dashed black lines, respectively. (b) Superposition of the HDAC6 CD1–Trichostatin A complex (monomer B, color-coded as in (a)) and the HDAC6 CD2–Trichostatin A complex (PDB 5WGI; monomer A, C = light gray (protein) or dark gray (inhibitor)). W78 of CD1 is conserved as W459 in CD2, and this residue adopts alternate conformations in CD1 (“in”) and CD2 (“out”). The “out” conformation of W459 at the mouth of the HDAC6 CD2 active site enables the binding of polyethylene glycol fragment PEG-821.

1  
2  
3 The 1.09 Å-resolution crystal structure of the HDAC6 CD1–AR-42 complex is the highest  
4 resolution structure of HDAC6 CD1 determined to date and exemplifies the high quality crystals  
5 that can be prepared with the simplified protein construct developed for the current study. This  
6 complex crystallizes in previously unobserved orthorhombic space group  $P2_12_12_1$  with one  
7 monomer in the asymmetric unit. The hydroxamate moiety of the inhibitor chelates the catalytic  
8  $Zn^{2+}$  ion nearly symmetrically ( $Zn^{2+} \cdots O1$  distance = 2.1 Å and  $Zn^{2+} \cdots O2$  distance = 2.2 Å)  
9 (Figure 3). The  $Zn^{2+}$ -bound hydroxamate C=O group additionally accepts a hydrogen bond from  
10 Y363, and the  $Zn^{2+}$ -bound hydroxamate N–O<sup>-</sup> group accepts a hydrogen bond from H192; the  
11 hydroxamate NH group donates a hydrogen bond to H193.



37 **Figure 3.** Polder omit map of the HDAC6 CD1–AR-42 complex (PDB 6UO3; inhibitor contoured at 5.0  $\sigma$ ;  
38 K330 contoured at 2.5  $\sigma$ ). Atoms are color-coded as follows: C = light blue (monomer A), light gray  
39 (symmetry mate), or wheat (inhibitor), N = blue, O = red,  $Zn^{2+}$  = gray sphere, and water molecules =  
40 smaller red spheres. Metal coordination and hydrogen bond interactions are indicated by solid and  
41 dashed black lines, respectively.

42  
43 The amide carbonyl oxygen in the capping group of AR-42 accepts a hydrogen bond  
44 from the side chain of S150. Interestingly, the corresponding residue also appears in HDAC6  
45 CD2 as S531, where it accepts a hydrogen bond from the backbone NH group of the scissile  
46 acetyllysine residue of the substrate.<sup>36</sup> These serine residues are unique to the active sites of  
47 HDAC6 CD1 and CD2 in comparison with other HDAC isozymes. Notably, HDAC6 CD2-  
48 selective inhibitors form hydrogen bonds with S531,<sup>36,38,40,42,43</sup> so S150 may similarly serve as a  
49 target in the design of HDAC6 CD1-selective inhibitors.

1  
2  
3 The amide carbonyl group of AR-42 forms two water-mediated hydrogen bonds in the  
4 active site of HDAC6 CD1: one with the side chain amino group of K330 and another to the  
5 imidazole N $\epsilon$ -H group of Zn<sup>2+</sup> ligand H232. Water-mediated hydrogen bonds with corresponding  
6 Zn<sup>2+</sup> ligand H614 of HDAC6 CD2 are similarly observed in the binding of certain inhibitors to this  
7 catalytic domain.<sup>36,38,40</sup> The phenyl capping group of the inhibitor is oriented toward H82 and  
8 P83, while the isopropyl group is oriented towards solvent. Notably, the benzyl group of AR-42  
9 is nestled in the aromatic crevice formed by W261 and F202 where it makes favorable offset  $\pi$ -  
10  $\pi$  interactions. This aromatic crevice contrasts with that of the CD2 domain, where it is defined  
11 by two phenylalanine residues (F583 and F643).<sup>39,40</sup>

12  
13  
14 The 1.27 Å-resolution crystal structure of the Y363F HDAC6 CD1–Trichostatin A  
15 complex contains two monomers in the asymmetric unit (Figure 4a). Crystals form in monoclinic  
16 space group *P*2<sub>1</sub> and are isomorphous with crystals of the wild-type enzyme-inhibitor complex.  
17 The amino acid substitution does not cause any significant structural rearrangements, and the  
18 rmsd of 300 C $\alpha$  atoms between the wild-type and Y363F HDAC6 CD1 structures is 0.16 Å. The  
19 phenolic hydroxyl group of Y363 is important for catalysis and inhibitor binding in metal-  
20 dependent deacetylases. However, absent a hydrogen bond interaction with Y363 in the Y363F  
21 variant, it is notable that inhibitor binding is otherwise generally identical to that observed in the  
22 active site of the wild-type enzyme (Figure 4b).

23  
24  
25 Even so, some structural differences are observed for certain active site residues. Most  
26 prominent is the 66° rotation of F363 compared with Y363 in the wild-type enzyme-inhibitor  
27 complex, suggesting flexibility for this residue (Figure 4b). A water molecule fills the void created  
28 by the conformational change of F363. This water molecule accepts a hydrogen bond from the  
29 backbone NH group of G362 and donates a hydrogen bond to the hydroxamate C=O group of  
30 Trichostatin A. Additionally, K330 is characterized by well-defined electron density, but it does  
31  
32  
33  
34  
35  
36  
37  
38  
39  
40  
41  
42  
43  
44  
45  
46  
47  
48  
49  
50  
51  
52  
53  
54  
55  
56  
57  
58  
59  
60

not form a hydrogen bond with the inhibitor. The dimethylamino moiety of the capping group also forms a water-mediated hydrogen bond with H82.

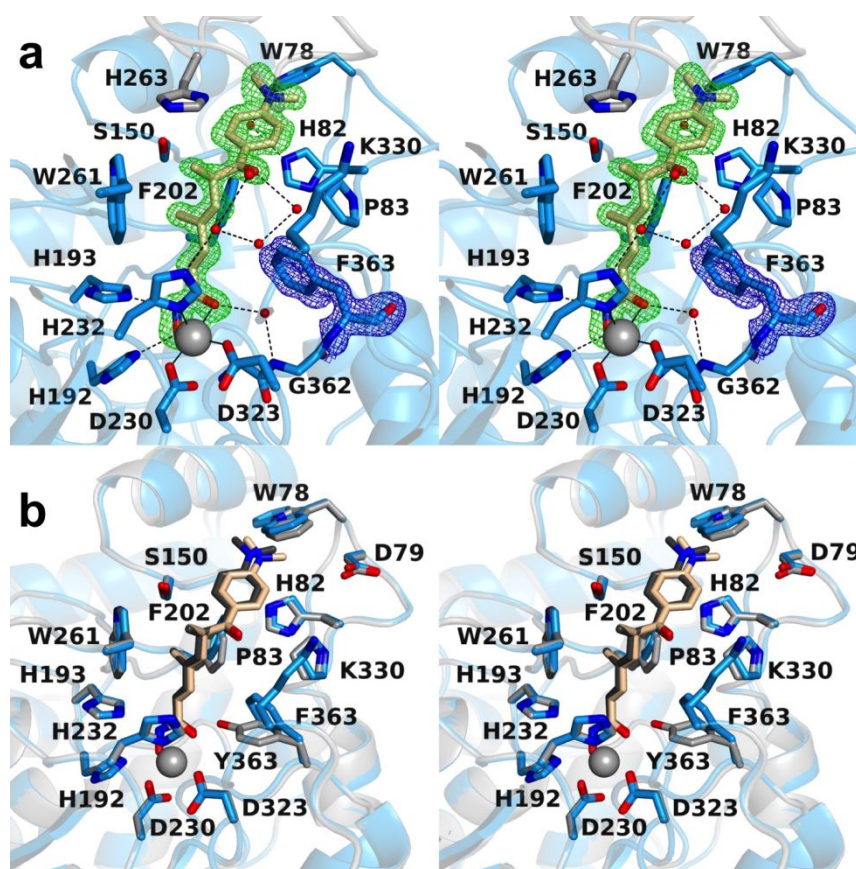
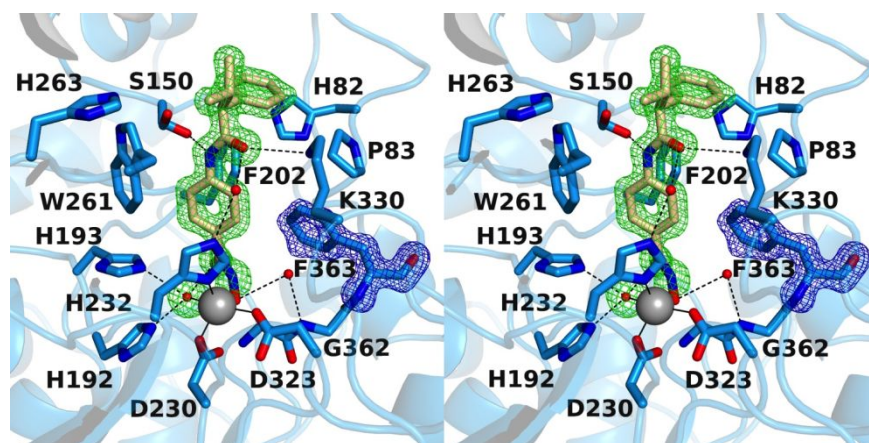


**Figure 4. (a)** Polder omit map of the Y363F HDAC6 CD1–Trichostatin A complex (PDB 6UO4; monomer A, contoured at  $4.5 \sigma$ ; F363 contoured at  $4.5 \sigma$ ). Atoms are color-coded as follows: C = light blue (monomer A), light gray (monomer B), or wheat (inhibitor), N = blue, O = red,  $Zn^{2+}$  = gray sphere, and water molecules = smaller red spheres. Metal coordination and hydrogen bond interactions are indicated by solid and dashed black lines, respectively. **(b)** Superposition of the Y363F HDAC6 CD1–Trichostatin A complex (color-coded as in (a)) with the wild-type HDAC6 CD1–Trichostatin A complex (C = light gray (protein) or dark gray (inhibitor); PDB 6UO2). The inhibitor binding conformation is essentially identical in both structures and is not affected by the amino acid substitution.

The 1.44 Å-resolution crystal structure of the Y363F HDAC6 CD1–AR-42 complex contains one monomer in the asymmetric unit. Crystals form in orthorhombic space group  $P2_12_12_1$  and are isomorphous with crystals of the wild-type enzyme-inhibitor complex. The amino acid substitution does not cause any significant structural rearrangements, and the rmsd of 313 C $\alpha$  atoms between the wild-type and Y363F HDAC6 CD1 structures is 0.15 Å.

1  
2  
3 Intriguingly, however, hydroxamate-Zn<sup>2+</sup> coordination geometry is monodentate, with metal  
4 coordination achieved only by the hydroxamate N-O<sup>-</sup> group (Figure 5). A Zn<sup>2+</sup>-bound water  
5 molecule additionally forms a hydrogen bond with the carbonyl group of the hydroxamate  
6 molecule additionally forms a hydrogen bond with the carbonyl group of the hydroxamate  
7 moiety. This contrasts with bidentate hydroxamate-Zn<sup>2+</sup> coordination geometry in the wild-type  
8 enzyme-inhibitor complex (Figure 3). Possibly, the loss of the hydrogen bond between Y363  
9 and the hydroxamate carbonyl group in the Y363F mutant influences the denticity of  
10 hydroxamate-Zn<sup>2+</sup> coordination. A hydrogen bond with the phenolic hydroxyl group of Y363  
11 orients and activates the scissile carbonyl of acetyllysine for catalysis,<sup>23-25</sup> so it is conceivable  
12 that a hydrogen bond with Y363 also helps to orient the hydroxamate carbonyl of certain  
13 inhibitors.  
14  
15  
16  
17  
18  
19  
20  
21  
22 inhibitors.



23  
24  
25  
26  
27  
28  
29  
30  
31  
32  
33  
34  
35  
36  
37  
38  
39  
40 **Figure 5.** Polder omit map of the Y363F HDAC6 CD1-AR-42 complex (PDB 6UO5; contoured at 6.0  $\sigma$ ;  
41 F363 is contoured at 3.0  $\sigma$ ). Atoms are color-coded as follows: C = light blue (monomer A), light gray  
42 (symmetry mate), or wheat (inhibitor), N = blue, O = red, Zn<sup>2+</sup> = gray sphere, and water molecules =  
43 smaller red spheres. Metal coordination and hydrogen bond interactions are indicated by solid and  
44 dashed black lines, respectively.

45  
46 The side chain of F363 is rotated by 70° compared with Y363 in the wild-type enzyme-  
47 inhibitor complex (Figure 5). A water molecule occupies the resulting void, and this water  
48 molecule accepts a hydrogen bond from the backbone NH group of G362 and donates a  
49 hydrogen bond to the Zn<sup>2+</sup>-bound hydroxamate N-O<sup>-</sup> group. Additionally, the side chain of S150  
50 adopts two alternative conformations, each of which is within hydrogen bonding distance to the  
51  
52  
53  
54  
55  
56  
57  
58  
59  
60

1  
2  
3 amide NH group of AR-42. Since K330 is unique to HDAC6 CD1 among all metal-dependent  
4 HDAC isozymes, hydrogen bond interactions with this residue – either direct or water-mediated  
5 – could be targeted in the development of HDAC6 CD1-specific inhibitors. As observed in the  
6 enzyme-inhibitor complex with the wild-type enzyme, the benzyl group of AR-42 is nestled in the  
7 aromatic crevice formed by W261 and F202 where it makes favorable offset  $\pi$ - $\pi$  interactions.  
8  
9  
10  
11  
12

13  
14 The 1.40 Å-resolution crystal structure of the K330L HDAC6 CD1–AR-42 complex  
15 contains one monomer in the asymmetric unit. Crystals form in orthorhombic space group  
16  $P2_12_12_1$  and are isomorphous with crystals of the wild-type enzyme-inhibitor complex. The  
17 amino acid substitution does not cause any significant structural rearrangements, and the rmsd  
18 of 334 C $\alpha$  atoms between the wild-type and K330L HDAC6 CD1 structures is 0.08 Å. The  
19 K330L substitution makes the active site more like that of HDAC6 CD2, and this substitution  
20 confers more relaxed substrate specificity.<sup>36</sup> Notably, K330L is located in the vicinity of the L1  
21 pocket, where in HDAC6 CD2 the majority of inhibitor capping groups bind.<sup>36,38-43</sup>  
22  
23  
24  
25  
26  
27  
28  
29  
30

31 The K330L substitution does not perturb the inhibitor binding conformation (Figure 6).  
32 Bidentate hydroxamate-Zn<sup>2+</sup> coordination geometry is retained, and the inhibitor capping group  
33 moiety binds in the same pocket as observed in complexes with wild-type and Y363F HDAC6  
34 CD1 complexes. Therefore, although L330 is not the naturally occurring residue in the active  
35 site of HDAC6 CD1, its substitution does not perturb inhibitor binding conformations. However,  
36 its substitution enables cocrystallization of HDAC6 CD1 with additional inhibitors that do not  
37 behave similarly well in cocrystallization experiments with wild-type HDAC6 CD1.  
38  
39  
40  
41  
42  
43  
44  
45  
46

47 The 1.58 Å-resolution crystal structure of the K330L HDAC6 CD1–Resminostat complex  
48 contains two monomers in the asymmetric unit of a second, new orthorhombic space group.  
49 Electron density for a single conformation L330 is well defined in both monomers (Figure 7). As  
50 observed in most of the structures of enzyme-inhibitor complexes described herein, the ionized  
51 hydroxamate moiety coordinates to Zn<sup>2+</sup> in bidentate fashion.  
52  
53  
54  
55  
56  
57  
58  
59  
60

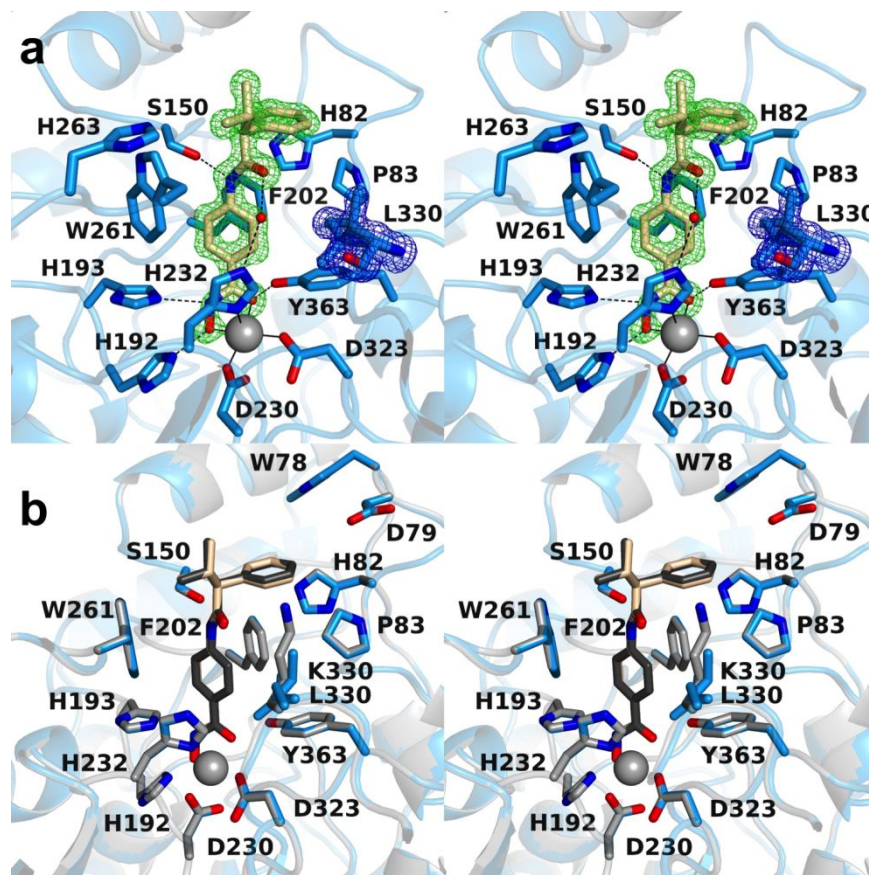


**Figure 6.** (a) Polder omit map of the K330L HDAC6 CD1-AR-42 complex (PDB 6UO7; contoured at 6.0  $\sigma$ ; L330 is contoured at 3.0  $\sigma$ ). Atoms are color-coded as follows: C = light blue (monomer A), light gray (symmetry mate), or wheat (inhibitor), N = blue, O = red,  $Zn^{2+}$  = gray sphere, and water molecules = smaller red spheres. Metal coordination and hydrogen bond interactions are indicated by solid and dashed black lines, respectively. (b) Superposition of the K330L HDAC6 CD1-AR-42 complex (color-coded as in (a)) with the wild-type HDAC6 CD1-AR-42 complex (C = light gray (protein) or dark gray (inhibitor); PDB 6UO3). The inhibitor binding conformation is essentially identical in both structures and is not affected by the amino acid substitution.

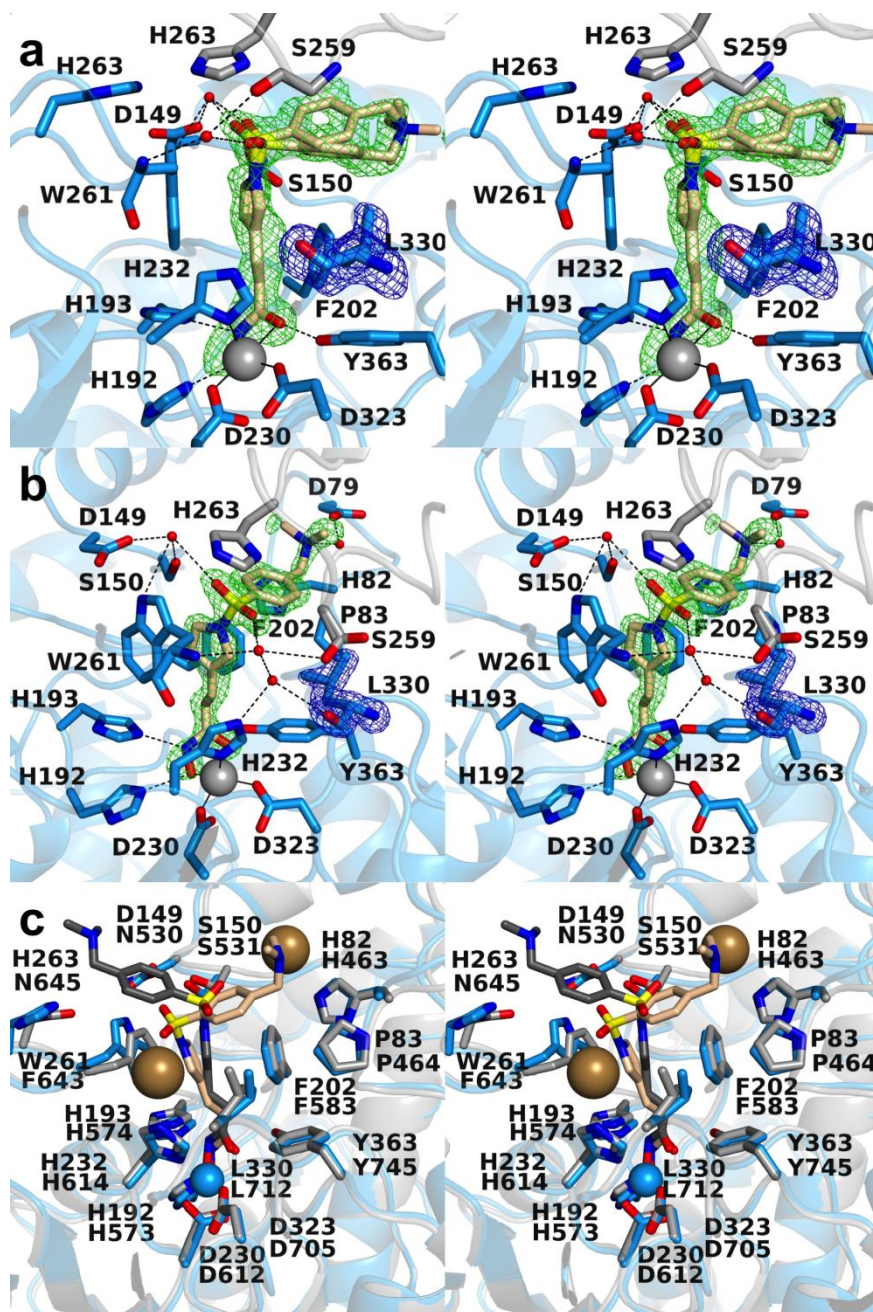


**Figure 7.** (a) Polder omit map of the K330L HDAC6 CD1–Resminostat complex (PDB 6UOB; monomer A, contoured at 3.5  $\sigma$ ). L330 is contoured at 3.5  $\sigma$ . Atoms are color-coded as follows: C = light blue (monomer A), light gray (monomer B), or wheat (inhibitor), N = blue, O = red, S = yellow, Zn<sup>2+</sup> = gray sphere, and water molecules = smaller red spheres. Metal coordination and hydrogen bond interactions are indicated by solid and dashed black lines, respectively. (b) Polder omit map of the K330L HDAC6 CD1–Resminostat complex (PDB 6UOB; monomer B, contoured at 5.0  $\sigma$ ). L330 is contoured at 3.5  $\sigma$ . Atoms are color-coded as follows: C = light blue (monomer B), light gray (symmetry mate), or wheat (inhibitor), N = blue, O = red, S = yellow, Zn<sup>2+</sup> = gray sphere, and water molecules = smaller red spheres. Metal coordination and hydrogen bond interactions are indicated by solid and dashed black lines, respectively. (c) Superposition of the K330L HDAC6 CD1–Resminostat complex (monomer B, color-coded as in (a)) and the wild-type HDAC6 CD2–Resminostat complex (monomer B, C = light gray (protein) or dark gray (inhibitor), I<sup>-</sup> = large sand-colored spheres; PDB 6PZR). The inhibitor capping group binds in alternate locations in each active site. The inhibitor binding conformation in the HDAC6 CD2 active site appears to be influenced by the binding of two iodide ions.

1  
2  
3 There is slight variation of enzyme-inhibitor interactions between monomers. The  
4 dimethylamino capping moiety is oriented toward F202 in both monomers. In monomer A, the  
5 dimethylamino group exhibits two alternative conformations separated by a 53° rotation. The  
6 sulfonyl group forms water-mediated hydrogen bonds with the backbone carbonyl of symmetry  
7 mate residue S259 in addition to forming water-mediated hydrogen bonds with D149, S150, and  
8 W261. In monomer B, the dimethylamino group exhibits only one conformation with a water-  
9 mediated hydrogen bond to D79. The sulfonyl group forms water-mediated hydrogen bonds to  
10 symmetry mate residue S259 in addition to forming water-mediated hydrogen bonds to D149,  
11 S150, H232, W261, and the backbone carbonyl of L330.  
12  
13  
14  
15  
16  
17  
18  
19  
20  
21

22 It is interesting to compare the binding conformation of Resminostat to HDAC6 CD2  
23 (PDB 6PZR) and K330L HDAC6 CD1. Superposition of the two structures shows that the  
24 inhibitor capping group occupies alternate locations in each structure (Figure 7c). Two iodide  
25 ions accompany inhibitor binding to HDAC6 CD2 and appear to influence the binding  
26 conformation of the capping group.  
27  
28  
29  
30  
31  
32

33 The 1.40 Å-resolution crystal structure of the K330L HDAC6 CD1–Givinostat complex  
34 contains one monomer in the asymmetric unit. Givinostat is the bulkiest inhibitor cocrystallized  
35 with HDAC6 CD1 to date and makes extensive interactions in the active site. The hydroxamate  
36 moiety coordinates to the catalytic Zn<sup>2+</sup> ion in characteristic bidentate fashion, and the aromatic  
37 ring of the phenylhydroxamate moiety nestles in the aromatic cleft defined by W261 and F202  
38 (Figure 8). While the diethylamino capping moiety is slightly disordered based on weak or  
39 broken electron density, the diethylamino group clearly donates a hydrogen bond with symmetry  
40 mate residue E97. Additional hydrogen bond interactions are observed between the inhibitor  
41 amide and S150 as well as a water-mediated hydrogen bond between the inhibitor amide and  
42 Zn<sup>2+</sup> ligand H232.  
43  
44  
45  
46  
47  
48  
49  
50  
51  
52  
53  
54  
55  
56  
57  
58  
59  
60

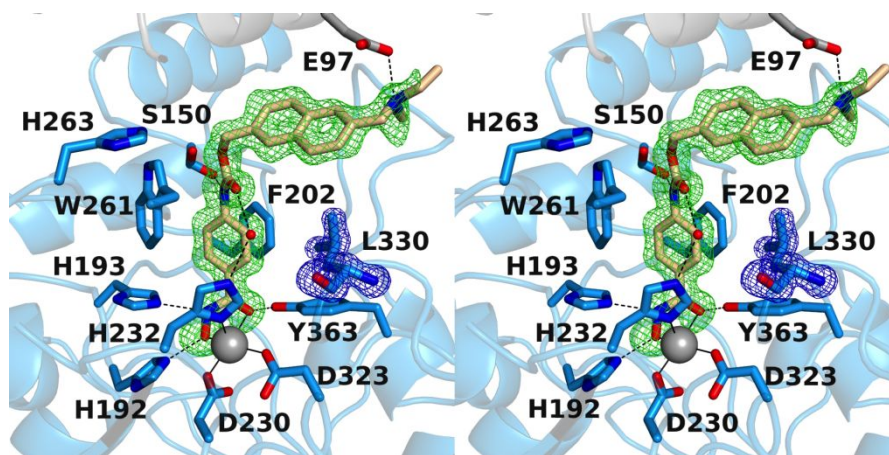


**Figure 8.** Polder omit map of the K330L HDAC6 CD1–Givinostat complex (PDB 6UOC; monomer A, contoured at  $3.0 \sigma$ ; L330 contoured at  $3.0 \sigma$ ). Atoms are color-coded as follows: C = light blue (monomer A), light gray (symmetry mate), or wheat (inhibitor), N = blue, O = red,  $Zn^{2+}$  = gray sphere, and water molecules = smaller red spheres. Metal coordination and hydrogen bond interactions are indicated by solid and dashed black lines, respectively.

**Catalytic activity measurements.** It has previously been demonstrated<sup>36</sup> that zebrafish HDAC6 CD1 and human HDAC6 CD1 exhibit optimal catalytic activity with substrates containing C-terminal acetyllysine residues such as  $Ac-GAK_{Ac}-CO_2^-$ . The measurement of steady-state kinetics with this substrate yields catalytic efficiencies ( $k_{cat}/K_M$ ) of  $8600 M^{-1}s^{-1}$  and  $1500 M^{-1}s^{-1}$  with zebrafish HDAC6 CD1 and human HDAC6 CD1, respectively. In comparison, using the corresponding amidated substrate  $Ac-GAK_{Ac}-CONH_2$ , catalytic efficiency with zebrafish HDAC6 CD1 is reduced to  $600 M^{-1}s^{-1}$ , and activity with human HDAC6 CD1 is reduced below measurable levels. Of note, the zebrafish enzyme exhibits much weaker catalytic activity with chromophoric substrates containing a C-terminal aminomethylcoumarin (AMC) moiety, such as  $Ac-RGK_{Ac}-AMC$ ; no catalytic activity is observed by the human enzyme with these substrates. This narrow substrate specificity is attributed to steric effects resulting from K330 in the HDAC6 CD1 active site.<sup>36</sup>

Here, based on specific activity measurements using the C-terminal acetyllysine substrates  $Ac-GAK_{Ac}-CO_2^-$  and  $Ac-AK_{Ac}-CO_2^-$ , we confirm as a positive control the narrow substrate specificity for maximal zebrafish HDAC6 CD1 activity. However, we also report weak

1  
2  
3 catalytic activity against substrates containing amino acid residues on the carboxyl side of the  
4 scissile acetyllysine residue (Table 2; due to weak specific activity measured for most  
5 substrates, we did not perform full steady-state kinetic analyses). Smaller residues, such as  
6 glycine or cysteine, but also including isoleucine, can be accommodated at this position in  
7 HDAC6 CD1 substrates. Even so, the observed catalytic activity against the best of these  
8 alternate substrates is at least 2–5-fold lower than that observed with Ac-AK<sub>Ac</sub> and Ac-GAK<sub>Ac</sub>.  
9  
10  
11  
12  
13  
14  
15

16 Peptides Ac-K<sub>Ac</sub>CGS-NH<sub>2</sub> and Ac-K<sub>Ac</sub>IGS-NH<sub>2</sub> derive from the HDAC6 substrate tau.<sup>28-30</sup>  
17  
18 The KXGS motifs are located within the microtubule-binding domain of tau and are important for  
19 microtubule stabilization.<sup>51</sup> While HDAC6 CD2 exhibits activity against these tau-derived  
20 substrates, it is interesting to note that HDAC6 CD1 exhibits comparable or better activity (Table  
21 2). While speculative, perhaps HDAC6 has two functional catalytic domains to enable  
22 simultaneous hydrolysis reactions with two different acetyllysine containing substrates, such as  
23 tau and the  $\alpha$ -domain of tubulin in the microtubule. It is unknown whether substrate binding and  
24 catalysis in one catalytic domain might influence substrate binding and catalysis in the other  
25 domain through some sort of allosteric effect. Although tau is thought to bind on the exterior of  
26 the microtubule,<sup>52</sup> some evidence suggests that it can also bind in the lumen of the  
27 microtubule,<sup>53</sup> where HDAC6 CD2 functions to deacetylate K40 of  $\alpha$ -tubulin.<sup>37,54</sup>  
28  
29  
30  
31  
32  
33  
34  
35  
36  
37  
38  
39  
40  
41  
42  
43  
44  
45  
46  
47  
48  
49  
50  
51  
52  
53  
54  
55  
56  
57  
58  
59  
60

**Table 2. Catalytic activity of HDAC6 CD1 and CD2 with selected peptide substrates**

Catalytic Domain	Substrate	Specific Activity (nmol product nmol <sup>-1</sup> enzyme min <sup>-1</sup> )
CD1	Ac-GAK <sub>Ac</sub>	62 ± 5
CD2	Ac-GAK <sub>Ac</sub>	11.0 ± 0.5
CD1	Ac-AK <sub>Ac</sub>	55 ± 4
CD2	Ac-AK <sub>Ac</sub>	20.0 ± 0.2
CD1	Ac-K <sub>Ac</sub> CGS-NH <sub>2</sub>	25 ± 2
CD2	Ac-K <sub>Ac</sub> CGS-NH <sub>2</sub>	8.0 ± 0.1
CD1	Ac-K <sub>Ac</sub> IGS-NH <sub>2</sub>	17 ± 1
CD2	Ac-K <sub>Ac</sub> IGS-NH <sub>2</sub>	16.0 ± 0.8
CD1	Ac-RGK <sub>Ac</sub> G-NH <sub>2</sub>	12 ± 1
CD1	Ac-GK GK <sub>Ac</sub> GS-NH <sub>2</sub>	12 ± 5
CD1	Ac-GK <sub>Ac</sub> GKGS-NH <sub>2</sub>	8 ± 1
CD1	Ac-GK GK <sub>Ac</sub> GS	5 ± 0.4
CD1	Ac-GK <sub>Ac</sub> GKGS	2 ± 0.2
CD1	Ac-LVK <sub>Ac</sub> G	7 ± 0.4
CD1	Ac-LVK <sub>Ac</sub> GI-NH <sub>2</sub>	1.00 ± 0.02
CD1	Ac-ELVK <sub>Ac</sub> GIL-NH <sub>2</sub>	1.00 ± 0.07
CD1	Ac-QPKK <sub>Ac</sub>	6 ± 1
CD1	Ac-TK <sub>Ac</sub> P	1.00 ± 0.07
CD1	Ac-K <sub>Ac</sub> KIET-NH <sub>2</sub>	1.0 ± 0.1
CD1	Ac-K <sub>Ac</sub> PVD-NH <sub>2</sub>	1.00 ± 0.01

All measurements represent mean ± average of absolute deviations from the mean in a given set of data. Ac-AK<sub>Ac</sub> and Ac-GAK<sub>Ac</sub> served as positive controls (K<sub>Ac</sub> = acetyllysine). All measurements were run in triplicate at 25° C.

Peptide Ac-RGK<sub>Ac</sub>G-NH<sub>2</sub> derives from cytoplasmic dynein 1 heavy chain 1.<sup>55,56</sup> Given that the linker between CD1 and CD2 in full-length human HDAC6 contains a dynein motor protein binding segment,<sup>18,19</sup> we were curious to see if HDAC6 CD1 might exhibit catalytic

1  
2  
3 activity against the dynein-based peptide or other peptides containing a  $-K_{Ac}G-$  segment.

4  
5 However, HDAC6 CD1 exhibits lower activity against these substrates.

## 6 7 **DISCUSSION**

8  
9  
10 HDAC6 is unique among all metal-dependent HDAC isozymes in that it contains two  
11 fully functional catalytic domains CD1 and CD2, and these catalytic domains exhibit striking  
12 differences in substrate specificity and inhibitor binding. While HDAC6 CD2 is the most-studied  
13 of the two, given its identification as a tubulin deacetylase<sup>26,27</sup> and as a tau deacetylase,<sup>28-30</sup> the  
14 biological function of HDAC6 CD1 has remained enigmatic. We expect that in-depth structural  
15 characterization of HDAC6 CD1 will further illuminate structure-function relationships that, in  
16 turn, will inform the design and development of selective inhibitors. As the first step toward this  
17 goal, we have presented an array of seven HDAC6 CD1–inhibitor complexes to facilitate the  
18 study of affinity interactions in the active site of HDAC6 CD1. While these inhibitors are “pan-  
19 HDAC” inhibitors, i.e., they are not particularly selective for the inhibition of HDAC6 over other  
20 HDAC isozymes, structural analyses of their complexes with HDAC6 nonetheless yield valuable  
21 information regarding potential interactions that could be targeted in the design of second-  
22 generation inhibitors with improved properties of affinity and selectivity.

23  
24  
25 The  $Zn^{2+}$  binding site and catalytic residues are identical in HDAC6 CD1 and CD2, so  
26 the chemical mechanism of amide bond hydrolysis must be identical in both catalytic domains:  
27 the  $Zn^{2+}$  ion and the catalytic tyrosine residue polarize the scissile carbonyl of acetyllysine for  
28 nucleophilic attack by a  $Zn^{2+}$ -bound water molecule, assisted by tandem histidine residues that  
29 serve general base-general acid functions.<sup>23-25</sup> However, there are nearby structural differences,  
30 including the aromatic crevice that accommodates the linker moiety of most inhibitors. In  
31 HDAC6 CD2, this crevice is formed by F583 and F643, whereas in HDAC6 CD1 this crevice is  
32 formed by F202 and W261. Since aromatic linkers of inhibitors bind in this crevice and make

1  
2  
3 favorable offset  $\pi$ - $\pi$  interactions, the slightly larger aromatic crevice of HDAC6 CD1 may be  
4  
5 capable of accommodating modified aromatic substituents.  
6

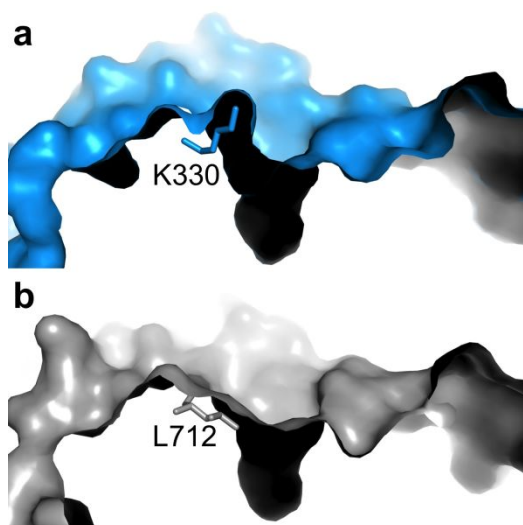
7  
8 On the opposite side of the aromatic crevice in the active site of HDAC6 CD1 is K330,  
9  
10 which confers specificity for acetyllysine substrates bearing a free  $\alpha$ -carboxylate group.<sup>36</sup> It is  
11  
12 thought that the additional steric bulk of this residue, in comparison with the leucine residue at  
13  
14 this position in HDAC6 CD2, accounts for differences in the binding conformations of  
15  
16 Trichostatin A to each catalytic domain (Figure 2b).<sup>36,37</sup> While the side chain of K330 is mainly  
17  
18 disordered in this complex (Figure 2a), its steric influence must nevertheless contribute to the  
19  
20 shift in the capping group of Trichostatin A. This shift is further accommodated by the  
21  
22 conformational difference observed for W78 in HDAC6 CD1 compared to HDAC6 CD2.  
23  
24

25  
26 Direct comparison of the active site contours of HDAC6 CD1 and CD2 reveals notable  
27  
28 differences that could impact inhibitor binding. For example, D149, H263, and W261 in HDAC6  
29  
30 CD1 appear as N530, N645, and F643 in HDAC6 CD2 (Figure 7c). An additional amino acid  
31  
32 substitution includes K330 in HDAC6 CD1, which appears as L712 in HDAC6 CD2 (Figure 9). It  
33  
34 is striking, too, that conformational differences in conserved residue W78/W459 also contribute  
35  
36 to differences in the active site contours. Overall, the active site cleft of HDAC6 CD1 is wider  
37  
38 than that of HDAC6 CD2, which contrasts with the narrow substrate specificity exhibited by  
39  
40 HDAC6 CD1. Since the K330L substitution relaxes this narrow substrate specificity,<sup>36</sup> K330  
41  
42 must play an important role in substrate binding; similarly, it could play an important role in  
43  
44 inhibitor binding and selectivity.  
45  
46

47  
48 With regard to inhibitor binding conformations in the active sites of wild-type and mutant  
49  
50 HDAC6 CD1 enzymes, it is important to note similar binding conformations regardless of  
51  
52 whether K330 is substituted with leucine (Figure 6b) or whether catalytic tyrosine Y363 is  
53  
54 substituted with phenylalanine (Figure 4b). Since we were unable to prepare crystalline  
55  
56 complexes of wild-type HDAC6 CD1 with all inhibitors described in this work, it is reassuring that  
57  
58  
59  
60

1  
2  
3 inhibitor cocrystallization studies with Y363F and K330L HDAC6 CD1 are likely to yield  
4 structures of complexes that are quite similar to those involving the wild-type enzyme.  
5  
6

7  
8 The specific activity measurements recorded in Table 2 confirm the narrow substrate  
9 specificity of zebrafish HDAC6 CD1, which exhibits maximal catalytic activity with acetyllysine  
10 substrates bearing a free  $\alpha$ -carboxylate group.<sup>36</sup> However, weaker catalytic activity is also  
11 observed for HDAC6 CD1 with substrates containing internal acetyllysine residues, such as Ac-  
12 K<sub>Ac</sub>CGS-NH<sub>2</sub>, which derives from the tau protein. The specific activity of HDAC6 CD1 with this tau-based  
13 substrate is only three-fold weaker than that measured with the best substrate, Ac-GAK<sub>Ac</sub>. Therefore, it is  
14 clear that zebrafish HDAC6 CD1 can accommodate substrates in which the scissile acetyllysine residue is  
15 flanked by smaller amino acids. This is consistent with the identification of human HDAC6 CD1 substrates  
16 containing internal acetyllysine residues using acetylome peptide microarrays in an elegant study  
17 reported by Barinka and colleagues.<sup>57</sup> Even so, our previously reported studies with a human HDAC6  
18 CD1-CD2 di-domain construct (with the CD2 domain inactivated by mutagenesis) indicate stricter  
19 substrate specificity for C-terminal acetyllysine residues compared with zebrafish HDAC6 CD1.<sup>36</sup> Since  
20 Barinka and colleagues used full-length human HDAC6 in their studies,<sup>57</sup> activity differences may result  
21 from the use of full-length human HDAC6 versus the truncated CD1-CD2 di-domain construct in enzyme  
22 assays.  
23  
24  
25  
26  
27  
28  
29  
30  
31  
32  
33  
34  
35  
36



54 **Figure 9. (a)** Molecular surface of HDAC6 CD1 (light blue). **(b)** Molecular surface of HDAC6 CD2 (light  
55 gray). Residues K330 and L712 differ between the catalytic domains, giving rise to different contours at  
56 the mouth of the active site.  
57  
58

## CONCLUDING REMARKS

While the precise biological function of HDAC6 CD1 remains unknown, the current study confirms our previous work<sup>36</sup> showing that catalytic activity exhibits very narrow substrate specificity, with maximal catalytic activity observed for acetyllysine substrates bearing a free  $\alpha$ -carboxylate group. Modification of the  $\alpha$ -carboxylate group by amidation, or peptide bond formation with an additional amino acid, compromises catalytic activity. Weak catalytic activity is measured with certain substrates bearing a smaller residue on the carboxyl side of acetyllysine, so the requirement for a free  $\alpha$ -carboxylate group on acetyllysine is not absolute for weak activity. The identification of glycine residues preceding the scissile acetyllysine residue in HDAC6 CD1 substrates identified in microarray analyses<sup>57</sup> is consistent with a general observation that smaller and flexible residues flanking acetyllysine appear to facilitate HDAC6 CD1 activity.

While the overall active site contour of HDAC6 CD1 is wider than that of HDAC6 CD2 (Figure 9), one side of the HDAC6 CD1 active site is constricted by K330. This residue contributes to the catalytic specificity for C-terminal acetyllysine substrates.<sup>36</sup> Our crystal structures reported herein show that K330 can interact with bound inhibitors, but it can also be disordered and thereby serve as a simple steric block. We cannot rule out the possibility that HDAC6 CD1 may utilize an as-yet undiscovered non-peptide substrate *in vivo*.

Structural differences between the active sites of HDAC6 CD1 and CD2, such as the aromatic crevice and the mouth of the active site in the vicinity of W78, lead to different binding orientations for Trichostatin A. While different binding conformations are also observed for Resminostat, binding to HDAC6 CD2 may also be influenced by two iodide ions that also bind in the active site of this complex. Nevertheless, sufficient structural differences are found in the active site of HDAC6 CD1 that could serve as the basis for the design and development of

1  
2  
3 isozyme-selective inhibitors. Such inhibitors could prove useful in elucidating the biological  
4  
5 function of HDAC6 CD1. We will report our results to this end in due course.  
6  
7  
8  
9  
10  
11  
12  
13  
14  
15  
16  
17  
18  
19  
20  
21  
22  
23  
24  
25  
26  
27  
28  
29  
30  
31  
32  
33  
34  
35  
36  
37  
38  
39  
40  
41  
42  
43  
44  
45  
46  
47  
48  
49  
50  
51  
52  
53  
54  
55  
56  
57  
58  
59  
60

## ASSOCIATED CONTENT

### Accession Codes

The atomic coordinates and crystallographic structure factors of CD1 complexes with the inhibitors shown in Figure 1 have been deposited in the Protein Data Bank ([www.rcsb.org](http://www.rcsb.org)) with accession codes as follows: HDAC6 CD1–Trichostatin A complex, 6UO2; HDAC6 CD1–AR-42 complex, 6UO3; Y363F HDAC6 CD1–Trichostatin A complex, 6UO4; Y363F HDAC6 CD1–AR-42 complex, 6UO5; K330L HDAC6 CD1–AR-42 complex, 6UO7; K330L HDAC6 CD1–Resminostat complex, 6UOB; K330L HDAC6 CD1–Givinostat complex, 6UOC.

## AUTHOR INFORMATION

### Corresponding Author

\*Tel.: 215-898-5714. E-mail: [chris@sas.upenn.edu](mailto:chris@sas.upenn.edu)

### ORCID

David W. Christianson: 0000-0002-0194-5212

### Funding

We thank the National Institutes of Health for grants GM49758 (D.W.C.) in support of this research.

### Notes

The authors declare no competing financial interests.

## Acknowledgments

We thank the Northeastern Collaborative Access Team (NE-CAT) beamlines, which are funded by the National Institute of General Medical Sciences from the National Institutes of Health (P30 GM124165). The Pilatus 6M detector on beamline 24-ID-C is funded by a NIH-ORIP HEI grant (S10 RR029205). This research used resources of the Advanced Photon Source, a U.S. Department of Energy (DOE) Office of Science User Facility operated for the DOE Office of Science by Argonne National Laboratory under Contract No. DE-AC02-06CH11357.

## References

1. Kouzarides, T. (2000) Acetylation: a regulatory modification to rival phosphorylation? *EMBO J.* **19**, 1176–1179.
2. Norvell, M. A. (2000) Rise of the rival. *Science* **327**, 964-965.
3. Choudhary, C., Kumar, C., Gnad, F., Nielsen, M. L., Rehman, M., Walther, T. C., Olsen, J. V., and Mann, M. (2009) Lysine acetylation targets protein complexes and co-regulates major cellular functions. *Science* **325**, 834-840.
4. López, J. E., Sullivan, E. D., and Fierke, C. A. (2016) Metal-dependent deacetylases: cancer and epigenetic regulators. *ACS Chem. Biol.* **11**, 706-716.
5. Zhao, S., Xu, W., Jiang, W., Yu, W., Lin, Y., Zhang, T., Yao, J., Zhou, L., Zeng, Y., Li, H., Li, Y., Shi, J., An, W., Hancock, S. M., He, F., Qin, L., Chin, J., Yang, P., Chen, X., Lei, Q., Xiong, Y., and Guan, K. L. (2010) regulation of cellular metabolism by protein lysine acetylation. *Science* **327**, 1000-1004.
6. Wang, Q., Zhang, Y., Yang, C., Xiong, H., Lin, Y., Yao, J., Li, H., Zhao, W., Yao, Y., Ning, Z. B., Zeng, R., Xiong, Y., Guan, K. L., Zhao, S., Zhao, G. P. (2010) Acetylation of metabolic enzymes coordinated carbon source utilization and metabolic flux. *Science* **327**, 1004-1007.
7. Choudhary, C., Weinert, B.T., Nishida, Y., Verdin, E., and Mann, M. (2014) The growing landscape of lysine acetylation links metabolism and cell signalling. *Nat. Rev. Mol. Cell Biol.* **15**, 536–550.
8. Berger S. L., Kouzarides, T., Shiekhhattar, R., and Shilatifard, A. (2009) An operational definition of epigenetics. *Genes Dev.* **23**, 781–783.
9. Delcuve, G. P., Khan, D. H., and Davie, J. R. (2012) Roles of histone deacetylases in epigenetic regulation: emerging paradigms from studies with inhibitors. *Clin. Epigenet.* **12**, 4-5.

- 1  
2  
3  
4  
5  
6 10. Arrowsmith, C. H., Bountra, C., Fish, P. V., Lee, K., and Schapira, M. (2012) Epigenetic  
7 protein families: a new frontier for drug discovery. *Nat Rev Drug Discov.* 11, 384–400.  
8  
9  
10 11. Falkenberg, K. J., and Johnstone, R. W. (2014) Histone deacetylases and their inhibitors in  
11 cancer, neurological diseases and immune disorders. *Nat Rev Drug Discov.* 13, 673–691.  
12  
13  
14 12. West, A. C., and Johnstone, R. W. (2014) New and emerging HDAC inhibitors for cancer  
15 treatment. *J. Clin. Invest.* 124, 30–39.  
16  
17  
18 13. Ma, N., Luo, Y., Wang, Y., Liao, C., Ye, W. C., and Jiang, S. (2015) Selective histone  
19 deacetylase inhibitors with anticancer activity. *Curr. Top. Med. Chem.* 16, 415–426.  
20  
21  
22 14. Dokmanovic, M., Clarke, C., and Marks, P. A. (2007) Histone deacetylase inhibitors:  
23 overview and perspectives. *Mol Cancer Res.* 5, 981–989.  
24  
25  
26 15. Richon, V. M., Webb, Y., Merger, R., Sheppard, T., Jursic, B., Ngo, L., Civoli, F., Breslow,  
27 R., Rifkind, R. A., and Marks, P. A. (1996) Second generation hybrid polar compounds are  
28 potent inducers of transformed cell differentiation. *Proc. Natl. Acad. Sci. U. S. A.* 93, 5705-5708.  
29  
30  
31 16. Marks, P. A. (2007) Discovery and development of SAHA as an anticancer agent.  
32 *Oncogene* 26, 1351-1356.  
33  
34  
35 17. Mann, B. S., Johnson, J. R., Cohen, M. H., Justice, R., and Pazdur, R. (2007) FDA approval  
36 summary: Vorinostat for treatment of advanced primary cutaneous T-cell lymphoma. *Oncologist*  
37 12, 1247-1252.  
38  
39  
40 18. Verdell, A., and Khochbin, S. (1999) Identification of a new family of higher eukaryotic  
41 histone deacetylases: coordinate expression of differentiation-dependent chromatin modifiers. *J.*  
42 *Biol. Chem.* 274, 2440-2445.  
43  
44  
45  
46  
47  
48  
49  
50  
51  
52  
53  
54  
55  
56  
57  
58  
59  
60

- 1  
2  
3 19. Grozinger, C. M., Hassig, C. A., and Schreiber, S. L. (1999) Three proteins define a class of  
4 human histone deacetylases related to yeast Hda1p. *Proc. Natl. Acad. Sci. U. S. A.* **96**, 4868-  
5 4873.  
6  
7  
8  
9  
10 20. Zhang, Y., Gilquin, B., Khochbin, S., and Matthias, P. (2006) Two catalytic domains are  
11 required for protein deacetylation. *J. Biochem.* **281**, 201-204.  
12  
13  
14 21. Zou, H., Wu, Y., Navre, M., and Sang, B. C. (2006) Characterization of the two catalytic  
15 domains in histone deacetylase 6. *Biochem. Biophys. Res. Commun.* **341**, 45-50.  
16  
17  
18  
19 22. Hook, S. S., Orián, A., Cowley, S. M., and Eisenman, R. N. (2002) Histone deacetylase 6  
20 binds polyubiquitin through its zinc finger (PAZ domain) and copurifies with deubiquitinating  
21 enzymes. *Proc. Natl. Acad. Sci. U. S. A.* **99**, 13425-13430.  
22  
23  
24  
25  
26 23. Lombardi, P. M., Cole, K. E., Dowling, D. P., and Christianson, D. W. (2011) Structure,  
27 mechanism, and inhibition of histone deacetylases and related metalloenzymes. *Curr. Opin.*  
28 *Struct. Biol.* **21**, 735-743.  
29  
30  
31  
32  
33 24. Wolfson, N. A., Pitcairn, C. A., and Fierke, C. A. (2013) HDAC8 substrates: histones and  
34 beyond. *Biopolymers* **99**, 112-126.  
35  
36  
37  
38 25. Porter, N.J., Christianson, D.W. (2019) Structure, mechanism, and inhibition of the zinc-  
39 dependent histone deacetylases. *Curr. Op. Struct. Biol.* **59**, 9-18.  
40  
41  
42  
43 26. Hubbert, C., Guardiola, A., Shao, R., Kawaguchi, Y., Ito, A., Nixon, A., Yoshida, M., Wang,  
44 X. F., and Yao, T. P. (2002) HDAC6 is a microtubule-associated deacetylase. *Nature* **417**, 455-  
45 458.  
46  
47  
48  
49 27. Zhang, Y., Li, N., Caron, C., Matthias, G., Hess, D., Khochbin, S., and Matthias, P. (2003)  
50 HDAC-6 interacts with and deacetylates tubulin and microtubules *in vivo*. *EMBO J.* **22**, 1168-  
51 1179.  
52  
53  
54  
55  
56  
57  
58  
59  
60

- 1  
2  
3 28. Min, S. W., Cho, S. H., Zhou, Y., Schroeder, S., Haroutunian, V., Seeley, W. W., Huang, E.  
4 J., Shen, Y., Masliah, E., Mukherjee, C., Meyers, D., Cole, P. A., Ott, M., and Gan, L. (2010)  
5 Acetylation of tau inhibits its degradation and contributes to tauopathy. *Neuron* 23, 953-966.  
6  
7  
8  
9  
10 29. Cohen, T. J., Guo, J. L., Hurtado, D. E., Kwong, L. K., Mills. I. P., Trojanowski, J. Q., Lee, V.  
11 M. (2011) The acetylation of tau inhibits its function and promotes pathological tau aggregation.  
12 *Nat Commun.* 2, 252.  
13  
14  
15  
16 30. Noack, M., Leyk, J., and Richter-Landsberg, C. (2014) HDAC6 inhibition results in tau  
17 acetylation and modulates tau phosphorylation and degradation in oligodendrocytes. *Glia* 62,  
18 535-547.  
19  
20  
21  
22  
23 31. Haggarty, S. J., Koeller, K. M., Wong, J. C., Grozinger, C. M., and Schreiber, S. L. (2003)  
24 Domain-selective small molecule inhibitor of histone deacetylase 6 (HDAC6)-mediated tubulin  
25 deacetylation. *Proc. Natl. Acad. Sci. U. S. A.* 100, 4389-4394.  
26  
27  
28  
29  
30 32. Zhang, Y., Gilquin, B., Khochbin, S., and Matthias, P. (2006) Two catalytic domains are  
31 required for protein deacetylation. *J. Biol. Chem.* 281, 2401-2404.  
32  
33  
34  
35 33. Zou, H., Wu, Y., Navre, M., and Sang, B.-C. (2006) Characterization of the two catalytic  
36 domains in histone deacetylase 6. *Biochem. Biophys. Res. Commun.* 341, 45-50.  
37  
38  
39  
40 34. Zhang, M., Xiang, S., Joo, H. Y., Wang, L., Williams, K. A., Liu, W., Hu, C., Tong, D.,  
41 Haakenson, J., Wang, C., Zhang, S., Pavlovicz, R. E., Jones, A., Schmidt, K, H., Tang, J.,  
42 Dong, H., Shan, B., Fang, B., Radhakrishnan, R., Glazer, P. M., Matthias, P., Koomen, J., Seto,  
43 E., Bepler, G., Nicosia, S. V., Chen, J., Li, C., Gu, L., Li, G. M., Bai, W., Wang, H., and Zhang,  
44 X. (2014) HDAC6 deacetylates and ubiquitinates MSH2 to maintain proper levels of MutSa. *Mol*  
45 *Cell* 55, 31-46.  
46  
47  
48  
49  
50  
51  
52  
53 35. Saito, M., Hess, D., Eglinger, J., Fritsch, A. W., Kreysing, M., Weinert, B. T., Choudhary, C.,  
54 and Matthias, P. (2019) Acetylation of intrinsically disordered regions regulates phase  
55  
56  
57  
58  
59  
60

1  
2  
3 separation. *Nat. Chem. Biol.* **15**, 51-61.  
4

5  
6 36. Hai, Y., and Christianson D. W. (2016) Histone deacetylase 6 structure and molecular basis  
7 of catalysis and inhibition. *Nat. Chem. Biol.* **12**, 741-747.  
8  
9

10  
11 37. Miyake, Y., Keusch, J. J., Wang, L., Saito, M., Hess, D., Wang, X., Melancon, B. J.,  
12 Helquist, P., Gut, H., and Matthias, P. (2016) Structural insights into HDAC6 tubulin  
13 deacetylation and its selective inhibition. *Nat. Chem. Biol.* **12**, 748-754.  
14  
15

16  
17 38. Porter, N. J., Mahendran, A., Breslow, R., and Christianson, D. W. (2017) Unusual zinc  
18 binding mode of HDAC6-selective hydroxamate inhibitors. *Proc. Natl. Acad. Sci. U. S. A.* **114**,  
19 13459-13464.  
20  
21  
22

23  
24 39. Porter, N. J., Wagner, F. F., and Christianson, D. W. (2018) Entropy as a driver of selectivity  
25 for inhibitor binding to histone deacetylase 6. *Biochemistry* **57**, 3916-3924.  
26  
27

28  
29 40. Porter, N. J., Osko, J. D., Diedrich, D., Kurz, T., Hooker, J. M., Hansen, F. K., and  
30 Christianson, D. W. (2018) Histone deacetylase 6-selective inhibitors and the influence of  
31 capping groups on hydroxamate-zinc denticity. *J. Med. Chem.* **61**, 8054-8060.  
32  
33

34  
35 41. Porter, N. J., Shen, S., Barinka, C., Kozikowski, A. P., and Christianson, D. W. (2018)  
36 Molecular basis for the selective inhibition of histone deacetylase 6 by a mercaptoacetamide  
37 inhibitor. *ACS Med. Chem. Lett.* **9**, 1301-1305.  
38  
39  
40

41  
42 42. Bhatia, S., Krieger, V., Groll, M., Osko, J. D., Reßing, N., Ahlert, H., Borkhardt, A., Kurz, T.,  
43 Christianson, D. W., Hauer, J., and Hansen, F. K. (2018) Discovery of the first-in-class dual  
44 histone deacetylase-proteasome inhibitor. *J. Med. Chem.* **61**, 10299-10309.  
45  
46  
47

48  
49 43. Mackwitz, M. K. W., Hamacher, A., Osko, J. D., Held, J., Schöler, A., Christianson, D. W.,  
50 Kassack, M. U., and Hansen, F. K. (2018) Multicomponent synthesis and binding mode of  
51 imidazo[1,2- $\alpha$ ]pyridine-capped selective HDAC6 inhibitors. *Org. Lett.* **20**, 3255-3258.  
52  
53  
54  
55  
56  
57  
58  
59  
60

- 1  
2  
3 44. Winn, M. D., Ballard, C. C., Cowtan, K. D., Dodson, E. J., Emsley, P., Evans, P. R., Keegan,  
4  
5 R. M., Krissinel, E. B., Leslie, A. G. W., McCoy, A., McNicholas, S. J., Murshudov, G. N., Pannu,  
6  
7 N. S., Potterton, E. A., Powell, H. R., Read, R. J., Vagin, A., and Wilson, K. S. (2011) Overview  
8  
9 of the CCP4 suite and current developments. *Acta Cryst. D67*, 235–242.  
10  
11  
12 45. Battye, T. G. G., Kontogiannis, L., Johnson, O., Powell, H. R., and Leslie, A. G. W. (2011)  
13  
14 iMOSFLM: a new graphical interface for diffraction image processing with MOSFLM. *Acta Cryst.*  
15  
16 *D67*, 271–281.  
17  
18  
19 46. Evans, P. R., and Murshudov, G. N. (2013) How good are my data and what is the  
20  
21 resolution? *Acta Cryst. D69*, 1204–1214.  
22  
23  
24 47. McCoy, A. J., Grosse-Kunstleve, R. W., Adams, P. D., Winn, M. D., Storoni, L. C., and  
25  
26 Read, R. J. (2007) Phaser crystallographic software. *J. Appl. Crystallogr.* *40*, 658–674.  
27  
28  
29 48. Emsley, P., Lohkamp, B., Scott, W. G., and Cowtan, K. (2010) Features and development of  
30  
31 Coot. *Acta Cryst. D66*, 486–501.  
32  
33  
34 49. Adams, P.D., Afonine, P.V., Bunkóczi, G., Chen, V.B., Davis, I. W., Echols, N., Headd, J. J.,  
35  
36 Hung, L., Kapral, G. J., Grosse-Kunstleve, R. W., McCoy, A. J., Moriarty, N. W., Oeffner, R.,  
37  
38 Read, R. J., Richardson, D. C., Richardson, J. S., Terwilliger, T. C., and Zwart, P. H. (2010)  
39  
40 PHENIX: a comprehensive Python-based system for macromolecular structure solution. *Acta*  
41  
42 *Cryst. D66*, 213–221.  
43  
44  
45 50. Chen, V. B., Arendall, W. B., III, Headd, J. J., Keedy, D. A., Immormino, R. M., Kapral, G. J.,  
46  
47 Murray, L. W., Richardson, J. S., and Richardson, D. C. MolProbity: all-atom structure validation  
48  
49 for macromolecular crystallography. *Acta Cryst. D66*, 12–21.  
50  
51  
52 51. Cook, C., Carlomagno, Y., Gendron, T.F., Dunmore, J., Scheffel, K., Stetler, C., Davis, M.,  
53  
54 Dickson, D., Jarpe, M., DeTure, M., and Petrucelli, L. (2014) Acetylation of the KXGS motifs in  
55  
56 tau is a critical determinant in modulation of tau aggregation and clearance. *Hum. Mol. Genet.*  
57  
58  
59  
60

1  
2  
3 23, 104-116.  
4

5  
6 52. Kadavath, H., Hofele, R. V., Biernat, J., Kumar, S., Tepper, K., Urlaub, H., Mandelkow, E.,  
7  
8 and Zweckstetter, M. (2015) Tau stabilizes microtubules by binding at the interface between  
9  
10 tubulin heterodimers. *Proc. Natl. Acad. Sci. U. S. A.* 112, 7501-7506.  
11

12  
13 53. Kar, S., Fan, J., Smith, M. J., Goedert, M., and Amos, L. A. (2003) Repeat motifs of tau bind  
14  
15 to the insides of microtubules in the absence of taxol. *EMBO J.* 22, 70-77.  
16

17  
18 54. Soppina, V., Herbstman, J. F., Skiniotis, G., and Verhey, K. J. (2012) Luminal localization of  
19  
20  $\alpha$ -tubulin K40 acetylation by cryo-EM analysis of Fab-labeled microtubules. *PLOS One* 7,  
21  
22 e48204.  
23

24  
25 55. Roberts, A. J., Kon, T., Knight, P. J., Sutoh, K., and Burgess, S. A. (2013) Functions and  
26  
27 mechanics of dynein motor proteins. *Nat. Rev. Mol. Cell Biol.* 14, 713-726.  
28

29  
30 56. Grotjahn, D. A., and Lander, G. C. (2019) Setting the dynein motor in motion: new insights  
31  
32 from electron tomography. *J. Biol. Chem.* 294, 13202-13217.  
33

34  
35 57. Kutil, Z., Skultetyova, L., Rauh, D., Meleshin, M., Snajdr, I., Novakova, Z., Mikesova, J.,  
36  
37 Pavlicek, J., Hadzima, M., Baranova, P., Havlinova, B., Majer, P., Schutkowski, M., Barinka, C.  
38  
39 (2019). The unraveling of substrate specificity of histone deacetylase 6 domains using  
40  
41 acetylome peptide microarrays and peptide libraries. *FASEB J.* 33, 4035-4045.  
42  
43  
44  
45  
46  
47  
48  
49  
50  
51  
52  
53  
54  
55  
56  
57  
58  
59  
60

For TOC use only:

